GA–A24144

OBSERVATION OF SUPRATHERMAL ELECTRONS DURING MAGNETIC RECONNECTION AT THE SAWTOOTH INSTABILITY IN DIII–D TOKAMAK

by
P.V. SAVRUKHIN and E.J. STRAIT

NOVEMBER 2002

DISCLAIMER

GA–A24144

OBSERVATION OF SUPRATHERMAL ELECTRONS DURING MAGNETIC RECONNECTION AT THE SAWTOOTH INSTABILITY IN DIII–D TOKAMAK

by
P.V. SAVRUKHIN* and E.J. STRAIT

This is a preprint of a paper to be submitted for publication in *Phys. Rev. Lett.*

*Nuclear Fusion Institute, RRC "Kurchatov Institute", Moscow, Russia.

Work supported by
the U.S. Department of Energy under
Contract No. DE-AC03-99ER54463

GENERAL ATOMICS PROJECT 30033
NOVEMBER 2002

ABSTRACT

Intense bursts of x-ray and electron cyclotron emission are observed during sawtooth instabilities in high-temperature plasmas in the DIII-D tokamak. The bursts are initiated around the X-point of the $m = 1$, $n = 1$ magnetic island at the beginning of the sawtooth crash and are displaced to larger radii later during the temperature collapse. Reconstruction of the magnetic configuration using motional Stark effect (MSE) data and numerical simulations indicates that the bursts can be connected with suprathermal electrons (E_r ~ 30–40 keV) generated during reconnection of the magnetic field around the $q = 1$ surface.

Periodic flattening of the temperature and density profiles in the central part of plasma, called sawtooth oscillations, is a common feature of tokamak discharges. The sawtooth crashes are generally connected with the process of breaking and topological rearrangement of the magnetic field lines (magnetic reconnection) during growth of the helical magnetohydrodynamic (MHD) perturbations around the $q = 1$ surface (here, $q = d\Psi_t/\Psi_p$, where Ψ_t, Ψ_p are toroidal and poloidal magnetic fluxes) [1]. Magnetic energy released by the reconnection could be transformed in part into acceleration of electrons to high suprathermal energies [2]. The appearance of electrons with non-thermal energies was in fact observed in studies of reconnection in various astrophysics phenomena (solar flares, earth's magnetosphere) [3] and laboratory experiments with relatively cold plasma [4,5]. However, electron acceleration during reconnection in high-temperature plasma, in conditions typically studied in experiments in tokamaks, has not been analyzed in detail so far. Theoretical studies have indicated, meanwhile, that in high-temperature plasma the reconnection process could be determined by the effects of finite electron inertia rather than classical resistive diffusion, and electron acceleration may play a dominant role in the reconnection process [6].

A significant result of the present work is the observation of suprathermal electrons (E_r ~ 30–40 keV) during magnetic reconnection at sawtooth crashes in high temperature plasmas in the DIII-D tokamak [7] (major radius R_0 = 1.75 m, minor radius a = 0.6 m), in discharges with auxiliary heating by neutral beam (NB) injection and fast wave radio frequency (rf) heating. Detailed documentation of these discharges is provided in [8]. While it was already shown in experiments that non-thermal electrons (E_r = 25–100 keV) can be generated in the presence of low-m, n MHD perturbations (here m, n – poloidal and toroidal mode numbers) [9,10,11] this is the first reported observation of suprathermal electrons in high temperature plasmas with simultaneous measurements of magnetic reconnection. Reconstruction of the internal magnetic fields in DIII-D plasmas is based on MSE measurements (up to 36 absolutely calibrated channels, time resolution δt = 2 ms) [12] and calculations of the equilibrium magnetic surfaces using the EFIT code [13] with additional constraints provided by the internal magnetic field measurements [14]. Non-thermal bursts and MHD perturbations are identified using a second harmonic X-mode ECE radiometer (spatial and time resolution are δr = 2.5 cm and δt = 0.01 ms) [10] and multi-array x-ray imaging systems placed at various angular positions around the torus (spatial and time resolution, δr = 3 cm and δt = 0.01 ms) [15].

Figure 1 shows a typical time evolution of the plasma parameters observed in experiments with deuterium plasma (upper-single null configuration with toroidal field B_T = 1.9 T, plasma current I_p = 1.2 MA, elongation κ_{95} = 1.7). Sawtooth oscillations are

initiated during the initial stage of NB injection (E_{NB} = 85 keV, P_{NB} = 2.8 MW) several hundred milliseconds after the current rise phase [t = 1.6 s in Fig. 1(a)]. The period of the sawteeth and amplitude of the central temperature modulation are considerably increased when rf heating (f = 60 MHz, P_{rf} = 1.0 MW) is combined with the NB injection [t = 1.8–3.0 s in Fig. 1(a)]. A typical sawtooth crash in such conditions is accompanied by intense bursts of electron cyclotron energy (ECE) emission, appearing during the last cycle of the m=1 mode rotation at the moment of the central temperature collapse [Fig. 1(b)]. The bursts are observed most clearly in the ECE channels whose second harmonic cold resonance layers are placed around and just outside the sawtooth inversion radius (q = 1 surface) at the low-field side of the torus. During the sawtooth crash the bursts are displaced to larger minor radius (Fig. 2). The rate of the burst displacement ($\Delta r/\Delta t$ ~ 1–2×10^4 m/s) is up to an order of magnitude faster than the "normal" propagation of heat pulses induced during the sawtooth crash [Figs. 1(b) and 2]. For simplicity, in Figs. 1 and 2 (and elsewhere in this paper) the ECE channels are labeled with the location of the low-energy second harmonic resonance, ignoring any relativistic frequency shift. However, the perturbations of the ECE emission outside the q = 1 surface appear to be shifted by up to Δr ~ 10 cm with respect to the x-ray perturbations (Fig. 2). This probably represents a relativistically downshifted cyclotron frequency related to the non-thermal electrons with energies E_r ~ 30–40 keV.

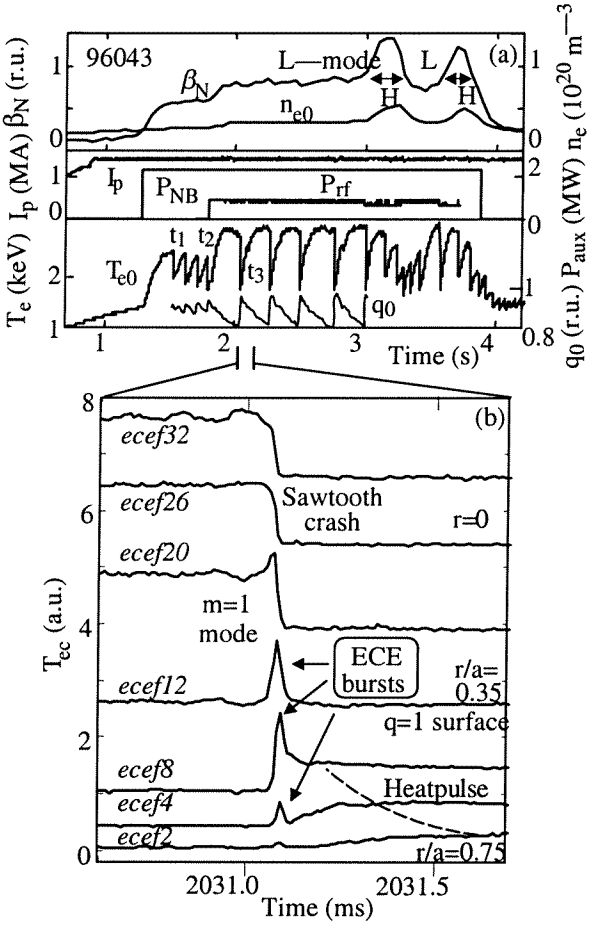

FIG. 1. (a) Time evolution of the plasma parameters in a DIII-D discharge with auxiliary heating by neutral beams (P_{NB} = 2.8 MW) and rf waves (P_{rf} = 1.0 MW). I_p is plasma current, β_N is normalized hydromagnetic pressure, n_e, T_e are central electron density and ECE temperature, q_0 is MSE safety factor at the plasma core. (b) Time evolution of the electron-cyclotron emission illustrating intense bursts of radiation during the sawtooth crash. The ECE channels are labeled with the location of the low-energy second harmonic resonance, neglecting any relativistic frequency shift.

Analysis of the ECE perturbations and measurements of the x-ray emission along various chords displaced around the torus in the poloidal and toroidal directions indicates that the appearance of non-thermal bursts coincides with the location of maximum perturbation due to the $m = 1$ mode [Figs. 1(b) and 3(a)]. Simulations of the chord-integrated x-ray intensity perturbations produced by the uniformly rotating $m = 1$ mode (solid displacement of the plasma core) superimposed with a bright "ribbon"-like structure around the $q = 1$ surface [Fig. 3(b)] suggest that the bursts can be associated with the position of the X-point of the magnetic island.

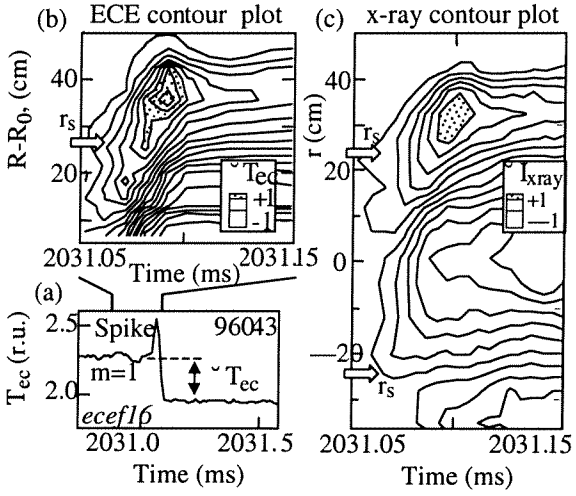

FIG. 2. Time evolution of electron-cyclotron emission in the central part of the DIII-D plasma (a) and contour plots of the ECE (b) and x-ray (c) perturbations during sawtooth crash. ECE and x-ray bursts (dashed areas) are observed at outer radii after a delay with respect to the perturbations around the $q = 1$ surface.

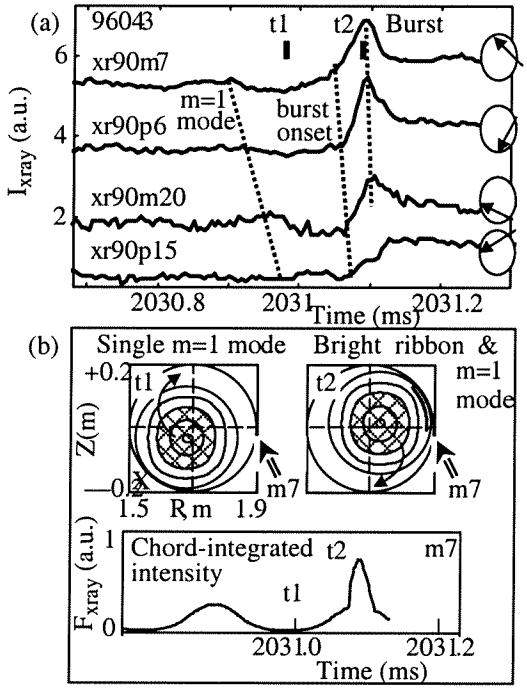

FIG. 3. (a) Time evolution of the x-ray intensity during a sawtooth crash measured along chords tangential to the $q = 1$ surface using x-ray arrays with various pitch angles: $\theta \approx 30$ deg (xr 90 m7), $\theta \approx -30$ deg (xr90p6), $\theta \approx -120$ deg (xr90m20), $\theta \approx -240$ deg (xr90p15). (b) Simulated images of the rotating $m = 1$ mode superimposed with a bright "ribbon"-like perturbation (appearing at t ~ 2031.06 ms) and "x-ray intensity" F_{x-ray} integrated along the line of sight of detector m7.

The bursts are observed most clearly in plasmas with auxiliary heating when a typical sawtooth crash is characterized by large amplitude ($\Delta T_e/T_e$ up to 50%) and fast time scale (t_{crash} ~ 0.05–0.1 ms) of the temperature collapse, while the amplitude of the $m = 1$, $n = 1$ precursor mode is relatively small. The bursts are sometimes observed during sawteeth in ohmically heated plasmas after switching off the auxiliary heating ($t > 3.88$ s in Fig. 1), during fast intermediate collapses in "compound" sawteeth, and during sawteeth in the H-mode confinement regime (t = 2.985–3.280 s and t = 3.350–3.770 s in Fig. 1). This indicates indirectly that conditions around the $q = 1$ surface during the crash rather than bulk plasma parameters are important in initiation of the bursts.

Generation of non-thermal electrons during a sawtooth crash could be represented by the following simplified process. Growth of the $m = 1$, $n = 1$ mode during a crash leads to squeezing of the magnetic field lines with different pitch angles around the $q = 1$ surface $\left(r = r_1\right)$. This is followed by formation of a narrow "current layer" where the plasma decouples from the magnetic field and reconnection takes place. Changes of magnetic topology are accompanied by formation of inductive electric fields and subsequent generation of non-thermal electron beams around the $q = 1$ surface. Simultaneous growth of magnetic field perturbations removes the non-thermal electrons from the reconnection layer to larger radii $\left(r > r_1\right)$ and effectively limits the density of the beams. As the non-thermal beams propagate toward larger minor radius, they are accompanied by bursts of non-thermal ECE and x-ray emission, with a delay at the outer radii.

The amplitude of the electric field induced during the reconnection can be estimated from the rate of change of the perturbed helical magnetic flux around the $q = 1$ surface. The electric field generated during a full reconnection is given approximately by $E_1 \sim \left(1 - q_0\right) r_1 B_{p1} / 4 t_{crash}$ [6], where t_{crash} is the duration of the sawtooth crash, q_0 is the safety factor at the plasma axis and B_{p1} is the poloidal magnetic field at the $q = 1$ surface prior to the sawtooth crash. Calculations indicate that electric fields of up to $E \sim$ 50 V/m can be predicted for the fast sawtooth crash (t_{crash} ~ 0.05 ms) shown in Fig. 4.

Production of non-thermal electrons depends at the first instant on the balance between electron acceleration in a strong electric field, $E > E_c$ [E_c is the critical electric field given by $E_c = e^3 n_e Z_{eff} \ell n \Lambda / \left(4\pi\varepsilon_0^2 m_e v_{th}^2\right)$] and the drag caused by Coulomb collisions (Dreicer effect [16]), and the knock-on avalanches due to close collisions of the electrons [17]:

$$\frac{dN_r}{dt} = \frac{n_e}{\tau_{dr}} + \frac{N_r}{\tau_{av}} - \frac{N_r}{\tau_{loss}} \quad ,$$

where, N_r and n_e are the density of the of the non-thermal electrons and the background plasma,

$$\tau_{dr}^{-1} \approx 0.3\nu_e \varepsilon_d^{-3\left(Z_{eff}+1\right)/16} \exp\left\{-1/\left(4\varepsilon_d\right) - \left[\left(Z_{eff}+1\right)/\varepsilon_d\right]^{1/2}\right\} ,$$

$\tau_{av} \approx 2m_e c\ell n\Lambda/eE$, $\varepsilon_d = E/E_c$, ν_e is the collision frequency of the electrons at the thermal velocity ν_{th}, and Z_{eff} is the effective plasma charge $\left(Z_{eff} \approx 1\right)$. The production of non-thermal electrons is balanced by losses due to macro-scale magnetic turbulence [18-21]: $\tau_{loss}^{-1} \approx D_m/\delta^2$, where $D_m = \left(\pi R_0 q \nu_r\right)\left(\delta B/B_T\right)^2$ is the magnetic diffusion coefficient, $\delta B/B_T = s_1 w_1^2/\left[16 r_1\left(R_0 + r_1\right)\right]$ is the amplitude of magnetic field perturbations, w_1 is the width of the $m=1$ magnetic island, s_1 is the magnetic shear around the $q=1$ surface $\left[s_1 \sim r/q\,(dq/dr)\right]$, δr is the scale-length $\left(\delta r \sim w_1\right)$, and v_r is the runaway electron mean velocity.

Typical results of the simulations for a set of the parameters represented in Table I are shown in Fig. 5(a). During a sawtooth crash at the time specified from experiments ($t \sim$ 2031.06–2031.11 ms) the electric field $\left(E_1\right)$ is gradually increased up to $E_{1max} \sim$ 50 V/m. This leads to generation of a runaway beam with density up to $N_{r1max} \sim 8.5\times10^{17}$ m^{-3} around the $q=1$ surface. Magnetic perturbations $\left(\delta B/B_T \sim 10^{-3}\right)$ during the crash produce an outward displacement of the runaway beam. (It is assumed in the simulations that $w_1 \sim 0.5 r_1$, and $\nu_r \sim 0.3c$). Switching-off of the strong electric field leads to decay of the non-thermal electron population. The simulated evolution of the electron beams agrees qualitatively with the temporal behavior of the ECE bursts observed in the experiments [Fig. 5(b)]. Calculations indicate that the production of non-thermal electrons is enhanced in plasmas with strong induced electric fields (during fast sawtooth crashes with large modification of the internal magnetic fields), while it is less pronounced in the presence of continuous MHD perturbations with saturated amplitude [22]. This agrees qualitatively with the increase in maximum amplitude of the ECE bursts observed in experiments with combined NB and rf heating [Fig. 5(c)]. It should be pointed out,

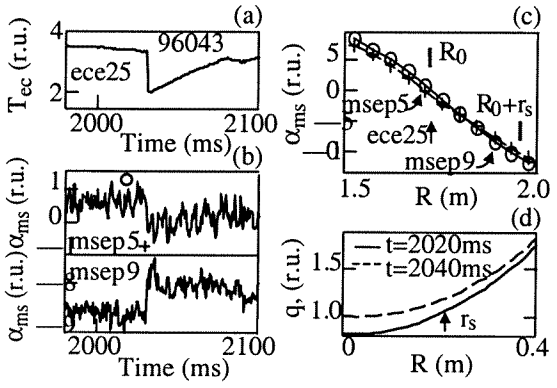

FIG. 4. Time evolution of the ECE emission (a) and MSE magnetic pitch angles (b) measured in the central part of the plasma. (c) Profiles of the magnetic pitch angle ($\alpha_{MSE} = B_z/B_T$, B_z is the vertical magnetic field) versus major radius prior to (solid) and after (dashed) sawtooth crash. (d) Radial profiles of the safety factor determined from MSE data using EFIT calculations ($r = a\rho$, where ρ is the normalized magnetic flux coordinate). Location of the sawtooth inversion radius r_s determined from the x-ray measurements is shown by the arrow.

Table I
Plasma Parameters Used in the Simulations of the Non-Thermal Electrons

	1st Crash	NB	NB and rf
Radius of the $q = 1$ surface, r_1 (m)	0.20	0.20	0.24
Crash time, t_{crash} (ms)	0.15	0.10	0.05
Safety factor changes, Δq_0 (r.u.)	0.04	0.06	0.17–0.20
Induced electric field, E_1 (V/m)	3	7	50
Electron temperature, T_{e1} (keV)	2.1	2.0	1.9
Electron density, n_{e1} (10^{19} m^{-3})	2.8	2.9	3.3
Dreicer field, E_e (V/m)	5.1	5.6	6.7
Magnetic shear, s_1 (r.u.)	0.8	0.8	0.8
Non-thermal density, N_{r1max} (10^{17} m^{-3})	2.5	4.5	8.5

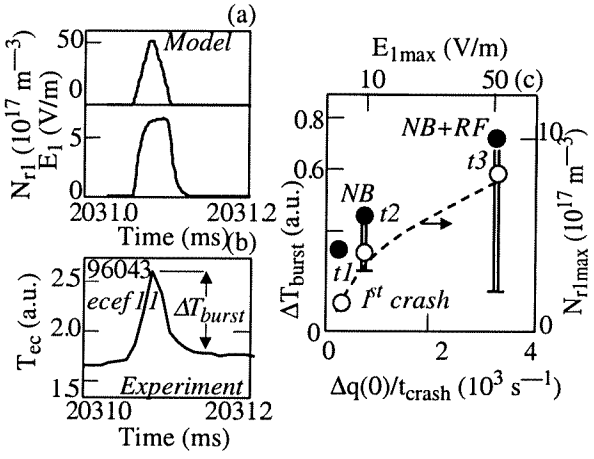

FIG. 5. (a) Calculated density $\left(N_{r1}\right)$ of the non-thermal electrons generated due to electric field E_1, induced around the $q = 1$ surface during the magnetic reconnection. (b) Time evolution of ECE emission, measured around the sawtooth inversion surface. (c) Maximum amplitude of ECE bursts (dark circles) observed in the experiments during sawtooth crashes with various rates of modification of the central safety factor [marks t1, t2, t3 in Fig. 1(a)]. Vertical double lines mark the range of amplitudes of smaller bursts observed in similar plasma conditions. Open circles represent the maximum density of non-thermal electrons $\left(N_{r1max}\right)$ calculated for parameters specified from the experiments (Table I.).

however, that in spite of agreement with the experimental observations the simulations represent an oversimplified model of the particle acceleration during magnetic reconnection. Detailed modeling of the magnetic reconnection [23,24] as well as measurements of the temporal evolution of the internal magnetic fields during a sawtooth crash are essential for a further analysis of the phenomena.

This work was supported in part by Russian Fund of Basic Research (Grant RFBR-00-02-16768) and the U.S. Department of Energy under Contract No. DE-AC03-99ER54463.

The authors would like to thank W.W. Heidbrink, T.E. Evans, E.A. Lazarus, S.V. Mirnov, B.W. Rice, and I.B. Semenov for stimulating discussions. The first author would like to thank General Atomics for hospitality during his visit to the Laboratory.

[1] B. B. Kadomtsev, *Tokamak plasma: A complex physical system* (IOP Publishing Ltd., Bristol, 1992).
[2] D. Biskamp, *Nonlinear magnetohydrodynamics* (Cambridge University Press, Cambridge, 1993).
[3] E. R. Priest, *Solar Magnetohydrodynamics* (Reidel, Dordrecht, 1984).
[4] A. G. Frank, Plasma Physics and Controlled Fusion **41**, A687 (1999).
[5] M. Yamada *et al.,* Phys. Plasmas **1**, 3269 (1994).
[6] J. A. Wesson, Nucl. Fusion **30**, 2545 (1990).
[7] J. L. Luxon, Nucl. Fusion **42**, 614 (2002).
[8] W. W. Heidbrink, E. D. Fredrickson, T. K. Mau, *et al.*, Nucl. Fusion **39**, 1369 (1999).
[9] G. Taylor *et al.,* Nucl. Fusion **32**, 1867 (1992).
[10] Ch. Fuchs, M. E. Austin, Phys.Plasmas **8**, 1594 (2001).
[11] P. V. Savrukhin, Phys. Rev. Lett. **86**, 3036 (2001).
[12] B. W. Rice, D. G. Nilson, and D. Wroblewski, Rev. Sci. Instrum. **66**, 373 (1995).
[13] L. L. Lao, H. E. St.John, R. D. Stambaugh, A. G. Kellman, and W. P. Pfeiffer, Nucl. Fusion **25**, 1611 (1985).
[14] L. L. Lao, J. R. Ferron, R. J. Groebner, W. Howl, H. E. St.John, E. J. Strait, and T. S. Taylor, Nucl. Fusion **30**, 1035 (1990).
[15] R. T. Snider, R. J. LaHaye, A. D. Turnbull, D. Wroblewski, Nucl. Fusion **34**, 483 (1994).
[16] H. Dreicer, Phys. Rev. **117**, 329 (1960).
[17] M. N. Rosenbluth, S. V. Putvinski, Nucl. Fusion **37**, 1355 (1997).
[18] R. Yoshino, S. Tokuda, Nucl. Fusion **40**, 1293 (2000).
[19] H. E. Mynick, J. D. Strachan, Phys. Fluids **24**, 695 (1981).
[20] R. Jaspers, N. J. Lopes Cardozo, F. C. Schuller, K. H. Finken, T. Grewe, G. Mank, Nucl. Fusion **36**, 367 (1996).
[21] P. Helander, L.-G. Eriksson, F. Andersson, Phys. Plasmas **7**, 4106 (2000).
[22] P. V. Savrukhin, Phys. Plasmas **9**, 3421 (2002).
[23] B. N. Rogers, R. E. Denton, J. F. Drake, and M. A. Shay, Phys. Rev. Lett. **87**, 195004 (2001).
[24] W. Park, D. A. Monticello, E. D. Fredrickson, K. McGuire, Phys. Fluids B **3**, 507 (1991).